Chemical Engineering Journal 162 (2010) 171–177

Contents lists available at ScienceDirect

Chemical Engineering Journal

journal homepage: www.elsevier.com/locate/cej

# Efficient removal of organic contaminants by a visible light driven photocatalyst $Sr_6Bi_2O_9$

Yanqing Yang, Gaoke Zhang*, Shujie Yu, Xiong Shen

*Hubei Key Laboratory of Mineral Resources Processing and Environment, School of Resources and Environmental Engineering, Wuhan University of Technology, 122 Luoshi Road, Wuhan 430070, PR China*

ARTICLE INFO

*Article history:*
Received 22 November 2009
Received in revised form 30 March 2010
Accepted 12 May 2010

*Keywords:*
$Sr_6Bi_2O_9$
Bismuth
Sol–gel method
4BS
Visible light
Photocatalytic activity

ABSTRACT

$Sr_6Bi_2O_9$ powders were synthesized by a sol–gel method using $Bi(NO_3)_3{\cdot}5H_2O$ and $Sr(NO_3)_2$ as the starting materials and were characterized by X-ray diffraction (XRD), UV–vis diffuse reflectance spectrum (UV–vis DRS), Fourier transform infrared (FT-IR) spectrum and Raman spectrum. The as-prepared $Sr_6Bi_2O_9$ powders showed an efficient photocatalytic activity in the decomposition of 4BS dye (a widely used azo dye) and 4-nitrophenol (4-NP, a priority pollutant) under visible light irradiation ($\lambda > 400$ nm). TA-PL analysis reveals that $HO^{\bullet}$ was not the dominant photooxidant. The radical scavengers experiments indicated that the main active species was $O_2^{\bullet -}$ in the photocatalytic degradation of dye under visible irradiation. A possible photodegradation mechanism of organic pollutants by the visible light driven $Sr_6Bi_2O_9$ was discussed.



## 1. Introduction

In recent years, oxide semiconductor photocatalysts have attracted extensive attention because of their wide applications in solar energy conversion and environmental purification [1–5]. To date, $TiO_2$ has been proved to be one of the best photocatalysts for widespread environmental applications [1,6–8]. However, $TiO_2$ photocatalyst could only be activated by UV light ($\lambda < 380$ nm) due to its large energy band gap (3.2 eV). In order to extend the absorption region of $TiO_2$ to visible light, some kinds of surface modification methods, such as metal doping, nonmetal doping or ion-implanting, have been used to obtain visible light driven photocatalysts [9–12]. However, some doped materials often suffer from thermal instability [9], increased carrier-recombination centers, or the requirement of expensive ion-implantation equipments [13]. Therefore, many researchers have focused their efforts on the design and development of undoped, single-phase oxide photocatalysts working under visible light illumination [14–16]. However, in oxide semiconductors, the conduction band levels of small-band-gap semiconductors are usually low because the deep valence bands are formed by O 2p. This is a major problem in enhancing the photocatalytic activities of oxide semiconductors. Recently, it has been reported that the Bi-based oxide photocatalysts are potential candidates for the visible light driven photocatalysts. In these materials, the valence band maximum (VBM) contains Bi 6s and O 2p orbitals, which results in a largely dispersed hybridized valence band. Thus, Bi-based oxide semiconductors are easy to acquire a visible light responsive ability [14,17]. The typical efficient Bi-based photocatalysts are $BiVO_4$ [18–21], $CaBi_2O_4$ [22], $Bi_2WO_6$ [23,24], $Bi_2MoO_6$ [25], bismuth titanium oxides [26–28] and some Bi-based multiple-metal oxides [29–32].

In the present paper, we reported a novel Bi-based photocatalyst, $Sr_6Bi_2O_9$, which is active in the photocatalytic decomposition of 4BS and 4-NP in water under visible light irradiation. The absorption edge of the as-obtained sample is at ca. 530 nm, corresponding to the band gap energy of 2.34 eV. Terephthalic acid photoluminescence probing technique (TA-PL) was used to detect the formation of the $HO^{\bullet}$ radicals in the process of photodegradation [33,34], and a visible light photocatalytic mechanism was conjectured.

## 2. Materials and methods

### 2.1. Preparation

The $Sr_6Bi_2O_9$ powders were prepared by a sol–gel method. The process flow chart for the sample is shown in Fig. 1.

Bismuth nitrate ($Bi(NO_3)_3{\cdot}5H_2O$), strontium nitrate ($Sr(NO_3)_2$), citric acid (CA), ethylene glycol ($C_2H_6O_2$), ammonia water and ethylene diaminetetraacetic acid (EDTA) were used as starting chemical reagents. All of the reagents were analytical grade and were used without further purification.

* Corresponding author. Tel.: +86 27 87651816; fax: +86 27 87887445.
*E-mail address:* gkzhang@whut.edu.cn (G. Zhang).

1385-8947/$ – see front matter © 2010 Elsevier B.V. All rights reserved.
doi:10.1016/j.cej.2010.05.024

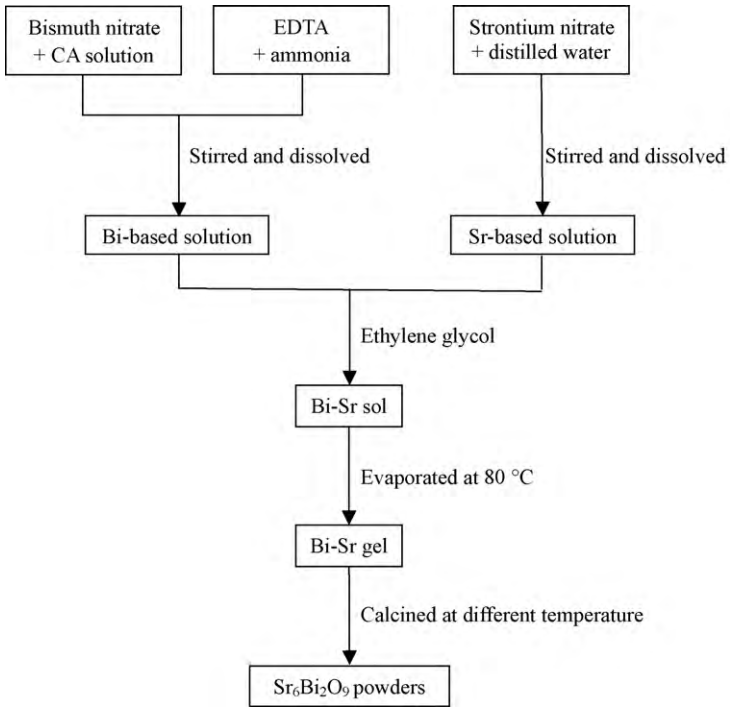


**Fig. 1.** The process flow chart for the preparation of $Sr_6Bi_2O_9$ powders.

Firstly, appropriate amounts of citric acid (CA) and $Bi(NO_3)_3{\cdot}5H_2O$ were added into distilled water at 80 °C under magnetic stirring, and then EDTA–ammonia solution was added slowly into the solution under continuous stirring until $Bi(NO_3)_3{\cdot}5H_2O$ was absolutely dissolved and the Bi–CA solution was obtained. Secondly, a $Sr(NO_3)_2$ solution in a molar ratio of 3:1 of Sr to Bi was added in the Bi–CA solution to prepare a homogeneous transparent aqueous solution. After being stirred for 30 min, ethylene glycol was added to promote citrate polymerization by polyesterification reaction [35]. In order to prevent precipitation, the precursor solution was prepared according to the molar ratio approximately 1:3 of Bi–Sr/CA, 3:2 of CA/EDTA and the pH was adjusted to 7.5 by using ammonia water. The mass ratio of the ethylene glycol to CA was 60:40. The as-obtained solution was stirred at 80 °C until it became transparent, and was then heated at 200–300 °C on electronic furnace until the amorphous polymeric precursors were formed. The precursors were calcined at 400 °C for 4 h at a heating rate of 10 °C $min^{-1}$ to promote the decomposition of organic matters, and then were ground and sintered at 800 °C for 6 h (the heating rates of 10 °C $min^{-1}$ from room temperature to 700 °C and 5 °C $min^{-1}$ from 700 °C to 800 °C were used, respectively). Finally, the $Sr_6Bi_2O_9$ powders were obtained.

### 2.2. Characterization

The structure and phase composition of the as-synthesized powders were characterized using X-ray powder diffraction (XRD) on a D/MAX-RB X-ray difractometer (Rigaku, Japan) equipped with Cu Kα radiation (λ = 1.5406 Å) and recorded with $2\theta$ ranging from 5° to 70°, while the accelerating voltage and the applied current were held at 40 kV and 50 mA, respectively. The Fourier transform infrared (FT-IR) spectra of the prepared powders were measured by the KBr pellet method with a Nexus Fourier transform infrared spectrometric analyzer. The Raman spectrum was recorded using a Renishaw invia spectrometer equipped with notch filter and a CCD detector. The absorption edge of the $Sr_6Bi_2O_9$ samples was measured by a UV–vis spectrophotometer (UV2550, Shimadzu, Japan). $BaSO_4$ was used as a reflectance standard in the UV–vis diffuse reflectance experiment. The $HO^{\bullet}$ trapping fluorescence spectra were taken on a fluorescence spectrophotometer (Shimadzu RF-5300PC). Total organic carbon (TOC) was measured by a TOC/TN multi analyzer (Multi N/C 2100, Analytik Jena, Germany).

### 2.3. Evaluation of photocatalytic activity

The photocatalytic activity of the $Sr_6Bi_2O_9$ powders was evaluated by the degradation of 4BS and 4-NP in aqueous solution under visible light irradiation. A 300 W Dy lamp was used as the light source with a 400 nm cutoff filter to ensure complete removal of radiation below 400 nm. For the degradation of 4BS, 0.05 g of photocatalyst was added into 50 mL of 4BS aqueous solution with a concentration of 30 mg/L. For the degradation of 4-NP, 0.2 g of the photocatalyst was added into 100 mL of 4-NP aqueous solution (5 mg/L). In each experiment, the suspensions were stirred in the dark for 5 min to disperse the catalyst prior to irradiation. At given time intervals, about 5 mL aliquots were sampled and centrifugated to remove the photocatalyst particles. Then the adsorption UV–vis spectrum of the centrifugated solution was recorded using a UV–vis spectrophotometer (Unico UV-2102PC). In the anaerobic study, the solution was deaerated by bubbling high pure $N_2$ during the decomposition process. For the adsorption measurement, 0.05 g of the as-prepared photocatalyst was added into 50 mL of 4BS aqueous solution with initial concentration of 5 mg/L, 20 mg/L, 30 mg/L, and 50 mg/L, respectively. The suspensions were stirred at room temperature in the dark to reach equilibrium, after centrifugated, the solution was taken to determine the 4BS concentration in the aqueous phase $C_{eq}$ by UV–vis spectrophotometer at 500 nm.

Our experimental results confirmed that the relationship between the absorbance and the concentration of 4BS aqueous solution could be described as the standard curve equation [36]:

$$A \approx 0.0231C \quad (1)$$

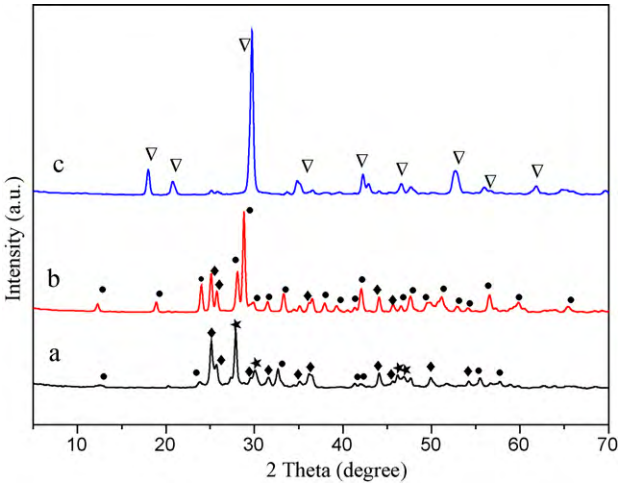


**Fig. 2.** XRD patterns of the $Sr_6Bi_2O_9$ sample calcined at (a) 400 °C, 4 h; (b) 700 °C, 6 h; (c) 800 °C, 6 h; (●) $Sr_2Bi_2O_5$; (♦) $SrCO_3$; (⋆) $Bi_2O_3$; (▽)$Sr_6Bi_2O_9$.

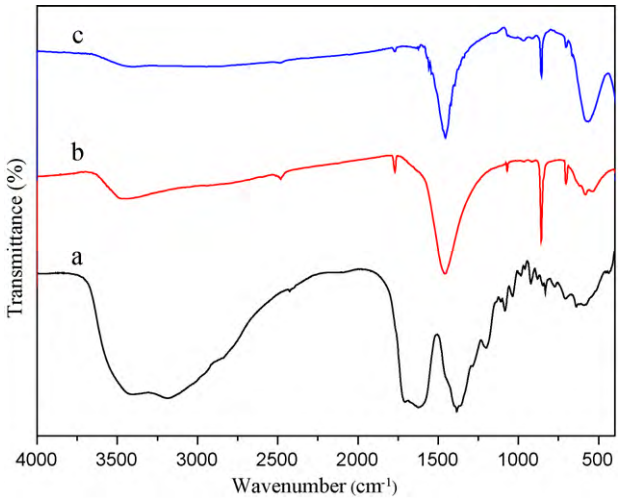


**Fig. 3.** FT-IR spectra of the precursors and powders calcined at different temperatures: (a) precursors; (b) 700 °C; (c) 800 °C.

So the 4BS degradation was calculated by the following equation:

$$\eta = \frac{C_0 - C}{C_0} \approx \frac{A_0 - A}{A_0} \quad (2)$$

where $C_0$ and $A_0$ are the initial concentration and absorbance of organic solutions at 500 nm corresponding to maximum absorption wavelength, $C$ and $A$ are the concentration and absorbance after visible light illumination, respectively.

## 3. Results and discussion

### 3.1. XRD analysis

Fig. 2 displays the XRD patterns of the $Sr_6Bi_2O_9$ powders prepared at different temperatures. As shown in Fig. 2, when the precursors were calcined at a lower temperature 400 °C for 4 h, a predominant phase $SrCO_3$, some $Bi_2O_3$ and little $Sr_2Bi_2O_5$ were formed. The sample prepared at 700 °C for 6 h was composed of the $Sr_2Bi_2O_5$ phase with orthorhombic structure (JCPDS Card: 39-1472) and a small amount of $SrCO_3$. All of the diffraction peaks of the sample prepared at 800 °C for 6 h can be indexed with the standard data of $Sr_6Bi_2O_9$ (JCPDS Card: 46-0498).

### 3.2. FT-IR absorption spectra

Fig. 3 gives the FT-IR spectra of the precursors and the powders annealed at different temperatures. It can be found that the intensity of the vibration peaks decreased during the conversion process of the precursors into the $Sr_6Bi_2O_9$ sample, which was due to the decomposition of the organic substance and the formation of the crystalline phase at the process of heat treatment. It has been known that –COOH group shows a group of absorption peaks at 3000–2500 $cm^{-1}$ [37]. However, these peaks were not observed in the FT-IR spectrum of the precursors. The absorption peak at 1706 $cm^{-1}$ in the FT-IR spectrum of the precursors is due to the symmetry and asymmetry flexing vibration of hydroxyl ($-COO^-$), which confirms the formation of metal citrate complexes in citrate precursors. As shown in Fig. 3, the intensity of the peaks between 400 $cm^{-1}$ and 800 $cm^{-1}$ increased with the increase of temperature, which indicates that the metal–oxide bond gradually formed [38].

### 3.3. Raman spectrum analysis

Raman spectrum of the $Sr_6Bi_2O_9$ sample prepared at 800 °C for 6 h is shown in Fig. 4. The Raman bands can be interpreted for four types [39,40]: acoustic Raman (AR) peaks in the low frequency region (less than 100 $cm^{-1}$); heavy metal (HM) peaks in the region 70–160 $cm^{-1}$; bridged anion (BA) peaks in the intermediate region (300–600 $cm^{-1}$) and non-bridged anion (NBA) peaks at higher frequencies.

In this study, Raman spectrum had been measured in the bridged and non-bridging regions of wavenumber between 200 $cm^{-1}$ and 2000 $cm^{-1}$. On the basis of the previous reports, the band at 621 $cm^{-1}$ can be attributed to the overlapping vibrations of Bi–O bonds in the distorted $BiO_6$ octahedral units [41].

A higher Raman stretching mode wavenumber indicates a more distorted structure, whereas a lower Raman stretching mode wavenumber reveals a more regular structure [42]. The as-prepared sample showed two peaks at 570 $cm^{-1}$ and 621 $cm^{-1}$, suggesting that $Sr_6Bi_2O_9$ has a distorted structure. The lattice distortion is one of the important parameters for charge separation and is beneficial for photodegradation, and thus enhancing the photocatalytic activity [43,44].

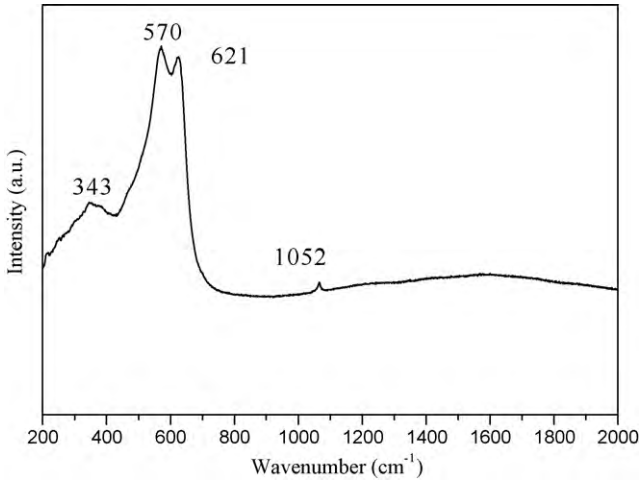


**Fig. 4.** Raman spectrum of the $Sr_6Bi_2O_9$ catalyst prepared by the sol–gel method at 800 °C for 6 h.

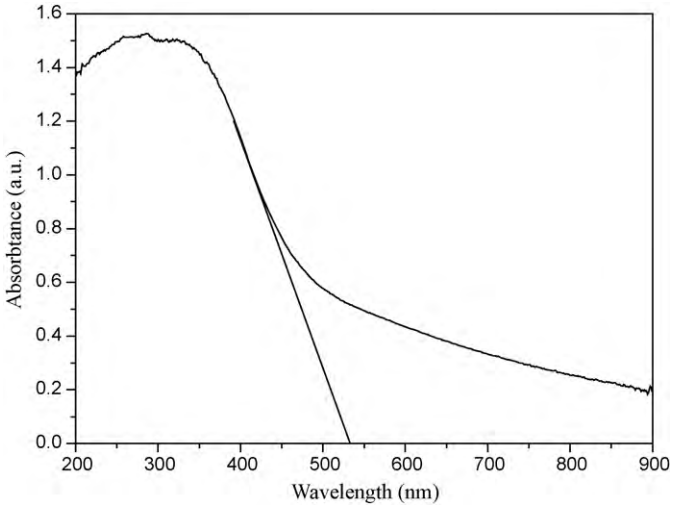


**Fig. 5.** UV–vis diffuse reflectance spectrum of the $Sr_6Bi_2O_9$ sample prepared by the sol–gel method at 800 °C for 6 h.

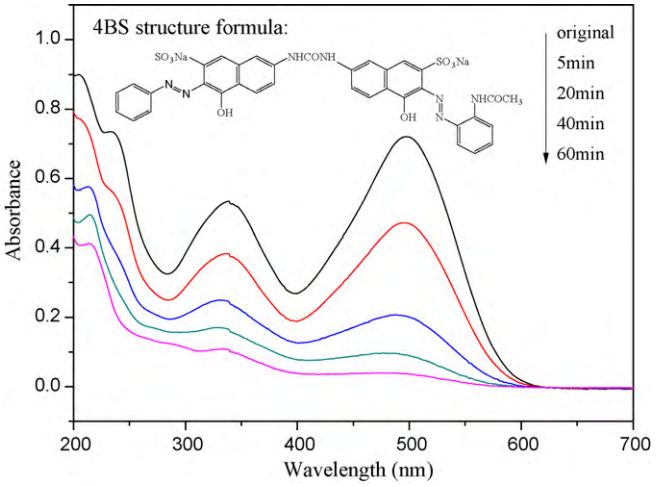


**Fig. 6.** UV–vis spectral changes of 4BS solution during the photocatalytic degradation by the as-prepared $Sr_6Bi_2O_9$ sample under visible light illumination.

### 3.4. UV–vis DRS analysis

The optical absorption property of the material and the migration of the light induced electrons and holes are considered as the most key factors controlling a photocatalytic reaction, which are relevant to the electronic structure characteristics of the material [22,45]. The photoabsorption ability of the material was detected by the UV–vis diffuse reflectance spectrum, as shown in Fig. 5. The $Sr_6Bi_2O_9$ powders showed the strong photoabsorption properties in the UV–vis light region. The band gap energy ($E_g$) of the material can be estimated by the formula [46]: $E_g = 1240/\lambda_g$, where $\lambda_g$ is the wavelength corresponding to the intersection point of the vertical and horizontal parts of the spectrum. From Fig. 5, the wavelength of the absorption edge of the as-prepared sample was 530 nm. Thus, the band gap energy estimated from the absorption edge was about 2.34 eV. This result indicates that the $Sr_6Bi_2O_9$ powders have a suitable band gap for photocatalytic decomposition of organic contaminants under visible light irradiation.

### 3.5. Photocatalytic properties

The photocatalytic degradation of 4BS dye (a kind of chemically stable and difficult decomposed dye) was used to investigate the photocatalytic activity of the $Sr_6Bi_2O_9$ catalyst prepared at 800 °C for 6 h. Fig. 6 illustrates the UV–vis absorption spectra of 4BS aqueous solution at different reaction times. The adsorption spectrum of the original solution showed four characteristic absorption spectra at 208 nm, 235 nm, 337 nm and 500 nm. The two absorption peaks at 208 nm and 235 nm belong to the structure of the benzene rings, the other two peaks correspond to the naphthalene rings and the nitrogen to nitrogen double bond (–N=N–), respectively. The absorption peak at $\lambda = 500$ nm decreased rapidly with increasing photocatalytic reaction time and almost disappeared after 60 min, indicating that the chromophore structure (–N=N–) of the azo dye was destroyed [47]. The characteristic peaks of naphthalene ring and benzene ring also became more smoothness after visible light irradiation for 60 min, and no new absorption spectra appeared in the visible and ultraviolet regions, which illuminates that the catalyst not only destroyed the chromophore of 4BS, but also decomposed the naphthalene ring and benzene ring partly. Fig. 7 displays the degradation of 4BS solution under different conditions. As shown in Fig. 7, a blank experiment in the absence of the photocatalyst under visible light irradiation shows that the photolysis of 4BS was negligible. However, with the as-prepared $Sr_6Bi_2O_9$ as the photocatalyst, 98% of 4BS was degraded after 60 min, showing the excellent photocatalytic activity of the as-prepared $Sr_6Bi_2O_9$ under visible light irradiation. Meanwhile, the adsorption of 4BS on the photocatalyst in the dark was also checked. After 60 min, approximately 23% of 4BS was adsorbed. This result showed that the as-prepared $Sr_6Bi_2O_9$ powders had a high adsorption capacity for 4BS, which was in favor of the photocatalytic decomposition of 4BS. Fig. 8 shows the adsorption isotherm of 4BS on $Sr_6Bi_2O_9$ catalyst at room temperature, the L-shape isotherm indicates that there was no strong competition between the solvent and the absorbate for the absorbent sites. As seen from the inset of Fig. 8, the adsorption isotherm was well represented by the Langmuir model. A linear relationship between $1/q_e$ and $1/C_e$ was observed, where $C_e$ represents the equilibrium bulk concentration of 4BS and $q_e$ is the amount of 4BS adsorbed onto the photocatalysts.

It is well-known that 4-NP is a priority aromatic compound and is difficult to be degraded in environment. To further investigate the photocatalytic property of the as-prepared $Sr_6Bi_2O_9$ powders, 4-NP was selected to evaluate the photocatalytic activity. Fig. 9 displays UV–vis spectral changes of 4-NP (5 mg/L) solution during the photocatalytic degradation by the as-prepared $Sr_6Bi_2O_9$ sample under visible light illumination. As shown in Fig. 9, an apparent decrease of 4-NP at the wavelength of 400 nm was observed, which indicates

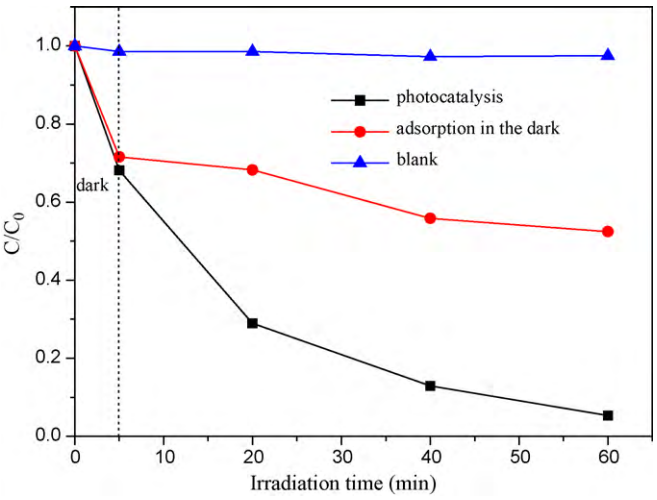


**Fig. 7.** The photodegradation efficiencies of 4BS solution as a function of irradiation time under different conditions.

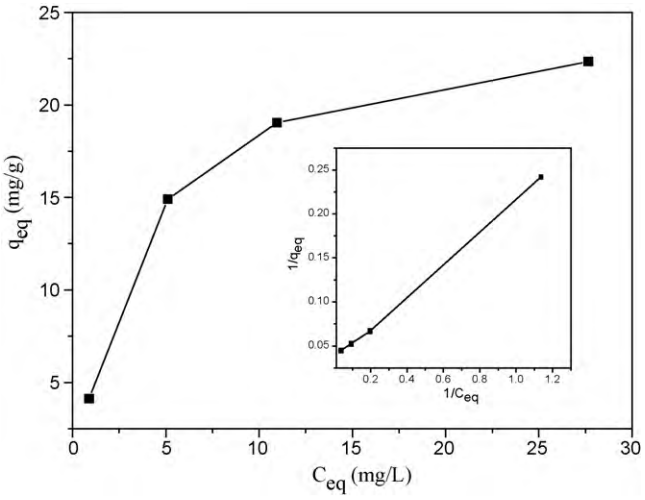


**Fig. 8.** The adsorption isotherm of 4BS on the as-prepared $Sr_6Bi_2O_9$ catalyst at room temperature.

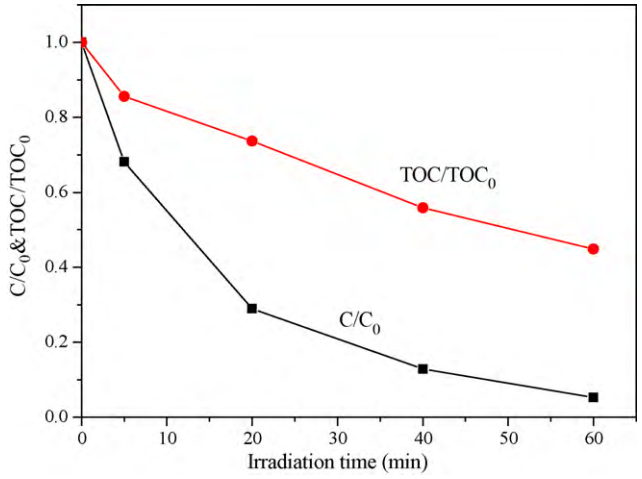


**Fig. 10.** The degradation and TOC removal of the 4BS solution under visible light illumination.

that the $Sr_6Bi_2O_9$ photocatalyst also showed an efficient photoactivity for the degradation of 4-NP under visible light irradiation ($\lambda > 400$ nm). From Figs. 6 and 9, the photocatalytic degradation rate of 4BS over the $Sr_6Bi_2O_9$ photocatalyst was higher than that of 4-NP. It can be attributed to the fact that the nitro group has high conjugated and resonance effects with the benzene ring which results in the high stability of 4-NP [48–50].

TOC removal of the 4BS and 4-NP solution are shown in Figs. 10 and 11, respectively. From Fig. 10, after a period of 60 min, the 4BS solution was completely decolored and 55.11% of TOC was removed. As shown in Fig. 11, 94.79% of 4-NP was degraded (analyzed at $\lambda = 400$ nm) and 30.73% of TOC of the 4-NP solution was removed after 8 h of irradiation. Clearly, the TOC removal of the 4BS solution and 4-NP solution was lower than the degradation (analyzed at the maximum wavelength) of 4BS and 4-NP, suggesting that the intermediates occurred during the photocatalytic process, this was in accordance with the absorption band shifting shown in Fig. 9 [51].

### 3.6. Visible light driven degradation mechanism

In the photocatalysis process of a semiconductor for the degradation of organic contaminants, photo-induced active species such as trapped holes, HO• radicals, peroxide radicals ($HO_2$•) and superoxide radical anions ($O_2$•$^-$) are suspected to be involved in the photocatalytic reaction. Terephthalic acid photoluminescence probing technique (TA-PL) has been widely used in the detection of HO• radicals. 2-Hydroxyl-terephthalic acid (TAOH), which is generated when terephthalic acid captures the HO• radicals, performs a strong fluorescence at around 426 nm on the excitation of its own 312 nm absorption band [33,34]. Therefore, the photoluminescence technique by TA-PL to detect the formation of the HO• radicals was conducted, and the intensity of the peaks increased slightly with the illumination time as shown in Fig. 12. This result indicates that the free HO• radicals could not be the main active oxygen species in the photochemical process. This phenomenon can be confirmed by the theoretical viewpoint. Generally, when the $Bi^{3+}$ ion forms a valence band, the holes formed by photoexcitation are regarded as $Bi^{5+}$ (or $Bi^{4+}$). Although a redox potential in an aqueous solution is different from that in solids, the standard redox potential of $Bi_2O_4/BiO^+$ ($Bi^{5+}/Bi^{3+}$) ($E^0 = +1.59$ eV at pH 0) could make sense for a rough estimation of the oxidation potential of the holes ($Bi^{5+}$) photogenerated in $Sr_6Bi_2O_9$ photocatalyst [52,23]. Therefore, it can be postulated that the hole photogenerated on the surface of $Sr_6Bi_2O_9$ could not react with $OH^-/H_2O$ to form HO• radicals because the standard redox potential of $Bi^{5+}/Bi^{3+}$ is more negative than that of HO•/$OH^-$ (+1.99) [53]. As mentioned above, the photocatalytic degradation of organic contaminant on $Sr_6Bi_2O_9$ could

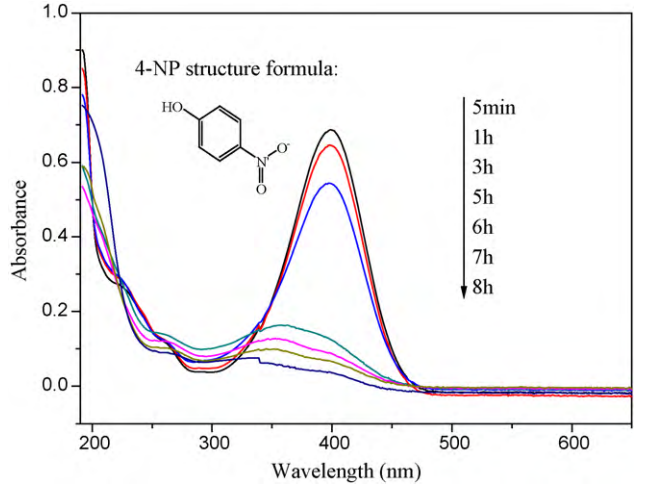


**Fig. 9.** UV–vis spectral changes of 4-NP (5 mg/L) solution during the photocatalytic degradation by the as-prepared $Sr_6Bi_2O_9$ sample under visible light illumination.

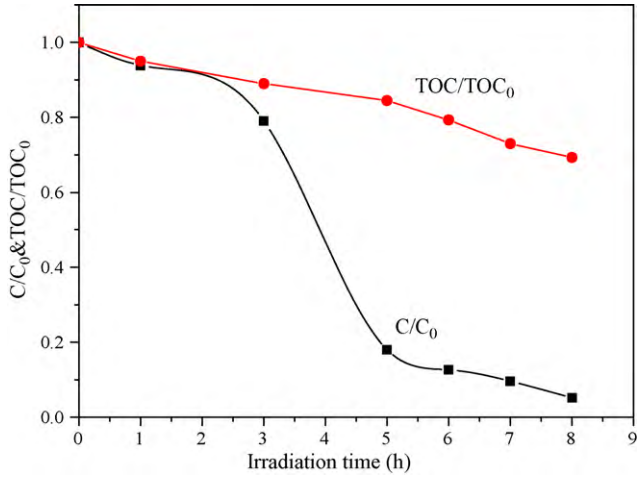


**Fig. 11.** The degradation and TOC removal of the 4-NP solution under visible light illumination.

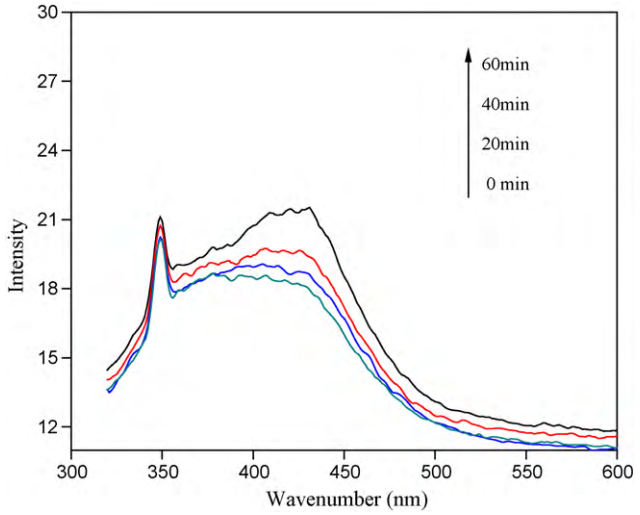


**Fig. 12.** HO• trapping PL spectra of $Sr_6Bi_2O_9$ on TA solution under visible irradiation.

be proceeded via direct reactions with holes trapped and superoxide radical anions ($O_2^{\bullet-}$). To further understand the effect of positive holes and $O_2^{\bullet-}$, the comparison experiments were performed between the original degradation curves of $Sr_6Bi_2O_9$/4BS dispersions with those obtained after addition of millimolar concentrations of quenchers in the initial solution, under otherwise identical conditions. From Fig. 13, it can be observed that KI (a quencher of positive hole and HO• radicals on catalyst surface [54,55]) did not affect the degradation rate of 4BS throughout the experiment. This result indicates that the direct holes were not the active oxidative species involved in the photodegradation process. However, addition of 2 mM of 1,4-benzoquinone (BQ, $C_6H_4O_2$, a quencher of $O_2^{\bullet-}$ [56]), the photodegradation efficiency of 4BS was apparently decreased, showing the $O_2^{\bullet-}$ was the main oxidative species responsible for the reduction of the 4BS dye solution. The generation of $O_2^{\bullet-}$ could be via photogenerated electron reacting directly with $O_2$ adsorbed on the surface of the catalyst. The anaerobic experiment was conducted to understand the effect of oxygen. As shown in Fig. 14, the photodegradation efficiency of 4BS was decreased apparently under the anoxic suspension ($N_2$-saturated condition). This result indicated that the presence of oxygen was responsible for the significant reduction of the 4BS solution, and its effect was to primarily act as an efficient electrons trap, leading to the generation of $O_2^{\bullet-}$ and preventing the recombination of electrons and holes [23]. Bandara and Kiwi [56] and Kondarides and co-workers [57] also showed that the main oxidative species was $O_2^{\bullet-}$ (or $HO_2^{\bullet}$) in the photocatalytic degradation of dye under visible irradiation.

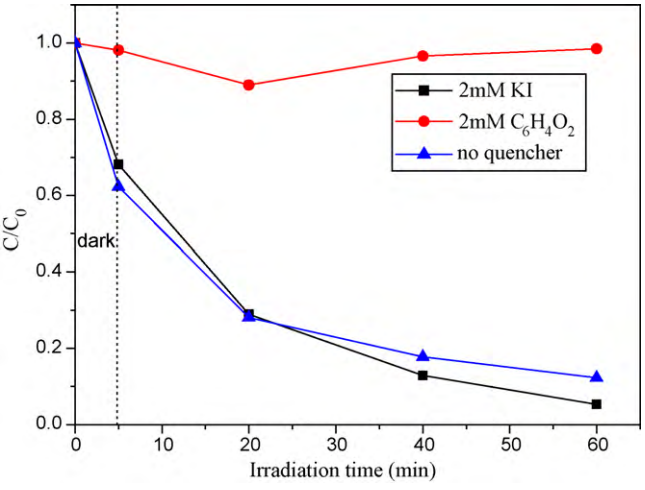


**Fig. 13.** Photocatalytic degradation of 4BS over the as-prepared $Sr_6Bi_2O_9$ photocatalyst under different solutions.

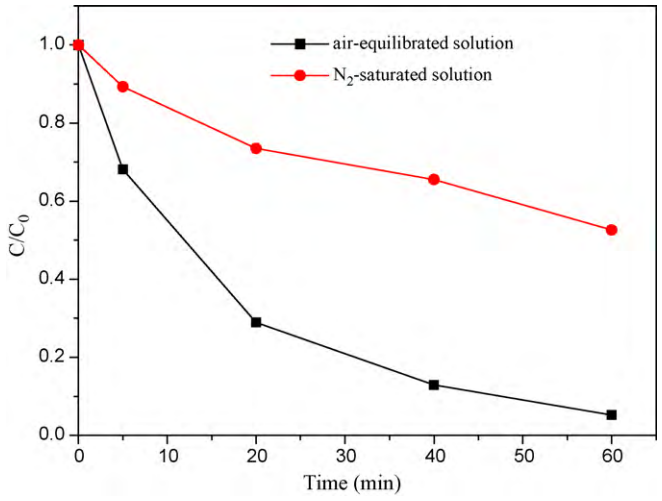


**Fig. 14.** Photocatalytic degradation of 4BS solution by the as-prepared $Sr_6Bi_2O_9$ sample in $N_2$-saturated and air-equilibrated solutions.

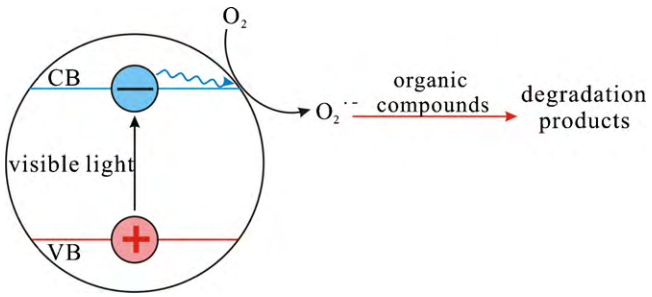


**Scheme 1.** Schematic illustrations of the $Sr_6Bi_2O_9$ photocatalytic reaction process under visible light irradiation. Minus and plus signs denote $e^-$ and $h^+$, respectively. CB and VB denote the conduction and valence bands of the $Sr_6Bi_2O_9$ particles, respectively. Wavy arrows represent the migration of charge carriers in the particles.

On the basis of the above experimental results, a possible mechanism for the dye photodegradation over $Sr_6Bi_2O_9$ could be proposed (Scheme 1). The photocatalyst could be efficiently stimulated to create electron–hole pairs under visible light irradiation which were long-lived enough to react with adsorbed $O_2$ to produce superoxide radical anions ($O_2^{\bullet-}$). The produced superoxide radical anions decomposed the organic contaminant to the final carbon dioxide and some inorganic products.

## 4. Conclusions

Visible light induced $Sr_6Bi_2O_9$ photocatalyst was prepared via a sol–gel method. The as-obtained $Sr_6Bi_2O_9$ powders showed a strong photoabsorption property from the UV light region to visible light and the band gap energy was about 2.34 eV. The as-prepared samples exhibited a high photocatalytic activity for the degradation of 4BS and 4-NP solutions. The photocatalytic reaction not only destroyed the chromophore of 4BS, but also decomposed the naphthalene ring and benzene ring partly. The HO• trapping PL studies suggested that HO• was not the dominant photooxidant in the $Sr_6Bi_2O_9$ photocatalysis. The superoxide radical anions ($O_2^{\bullet-}$) could take part in $Sr_6Bi_2O_9$ photocatalysis. The presence of oxygen was in favor of generating $O_2^{\bullet-}$ and preventing the recombination of electrons and holes.

## Acknowledgements

This work was supported by the Key Project of Chinese Ministry of Education (No.108164), National Basic Research Program of China (973 Program) 2007CB 613302, the National Natural Science Foundation of China (50872103) and the Project-sponsored by SRF for ROCS, SEM.

## References

[1] M.R. Hoffmann, S.T. Martin, W. Choi, D.W. Bahnemann, Environmental applications of semiconductor photocatalysis, J. Chem. Rev. 95 (1995) 69–96.
[2] S.F. Chen, W. Zhao, S.J. Zhang, W. Liu, Preparation, characterization and photocatalytic activity of N-containing ZnO powder, Chem. Eng. J. 148 (2009) 263–269.
[3] A. Fujishima, T.N. Rao, D.A. Tryk, Titanium dioxide photocatalysis, J. Photochem. Photobiol. C: Photochem. Rev. 1 (2000) 1–21.
[4] N. Wang, X.Y. Li, Y.X. Wang, X. Quan, G.H. Chen, Evaluation of bias potential enhanced photocatalytic degradation of 4-chlorophenol with $TiO_2$ nanotube fabricated by anodic oxidation method, Chem. Eng. J. 146 (2009) 30–35.
[5] J. Saien, M. Asgari, A.R. Soleymani, N. Taghavinia, Photocatalytic decomposition of direct red 16 and kinetics analysis in a conic body packed bed reactor with nanostructure titania coated Raschig rings, Chem. Eng. J. 151 (2009) 295–301.
[6] C. Wang, J.C. Zhao, X.M. Wang, B.X. Mai, G.Y. Sheng, P.A. Peng, J.M. Fu, Preparation, characterization and photocatalytic activity of nano-sized $ZnO_2/SnO_2$ coupled photocatalysts, Appl. Catal. B: Environ. 39 (2002) 269–279.
[7] A.L. Linsebigler, G.Q. Lu, J.T. Yates, Photocatalysis on $TiO_2$ surfaces: principles, mechanisms, and selected results, Chem. Rev. 95 (1995) 735–758.
[8] T. Torimoto, S. Ito, S. Kuwabata, H. Yoneyama, Effects of adsorbents used as supports for titanium dioxide loading on photocatalytic degradation of propyzamide, Environ. Sci. Technol. 30 (1996) 1275–1281.
[9] W. Choi, A. Termin, M.R. Hoffmann, The role of metal ion dopants in quantum-sized $TiO_2$: correlation between photoreactivity and charge carrier recombination dynamics, J. Phys. Chem. 98 (1994) 13669–13679.
[10] S.U.M. Khan, M. Al-Shahry, W.B. Ingler, Efficient photochemical water splitting by a chemically modified $n$-$TiO_2$, Science 297 (2002) 2243–2245.
[11] S. Sakthivel, H. Kisch, Daylight photocatalysis by carbon modified titanium dioxide, Angew. Chem. Int. Ed. 42 (2003) 4908–4911.
[12] W. Zhao, W.H. Ma, C.C. Chen, J.C. Zhao, Z.G. Shuai, Efficient degradation of toxic organic pollutants with $Ni_2O_3/TiO_{2-x}B_x$ under visible irradiation, J. Am. Chem. Soc. 126 (2004) 4782–4783.
[13] M. Anpo, Photocatalysis on titanium oxide catalysts approaches in achieving highly efficient reactions and realizing the use of visible light, Catal. Surv. Jpn. 1 (1997) 169–179.
[14] A. Kudo, K. Omori, H. Kato, A novel aqueous process for preparation of crystal form-controlled and highly crystalline $BiVO_4$ powder from layered vanadates at room temperature and its photocatalytic and photophysical properties, J. Am. Chem. Soc. 121 (1999) 11459–11467.
[15] A. Ishikawa, T. Takata, J.N. Kondo, M. Hara, H. Kobayashi, K. Domen, Oxysulfide $Sm_2Ti_2S_2O_5$ as a stable photocatalyst for water oxidation and reduction under visible light irradiation ($\lambda \leq 650$ nm), J. Am. Chem. Soc. 124 (2002) 13547–13553.
[16] H.G. Kim, D.W. Hwang, J.S. Lee, Single-phase oxide photocatalyst working under visible light, J. Am. Chem. Soc. 126 (2004) 8912–8913.
[17] M. Wiegel, W. Middel, G. Blasse, Influence of $ns^2$ ions on the luminescence of niobates and tantalates, J. Mater. Chem. 5 (1995) 981–983.
[18] S. Kohtani, M. Koshiko, A. Kudo, K. Tokumura, Y. Ishigaki, A. Toriba, K. Hayakawa, R. Nakagaki, Photodegradation of 4-alkylphenols using $BiVO_4$ photocatalyst under irradiation with visible light from a solar simulator, Appl. Catal. B: Environ. 46 (2003) 573–586.
[19] H. Harada, C. Hosoki, M. Ishikane, Sonophotocatalysis of water in a $CO_2$–Ar atmosphere, J. Photochem. Photobiol. A: Chem. 160 (2003) 11–17.
[20] S. Tokunaga, H. Kato, A. Kudo, Selective preparation of monoclinic and tetragonal $BiVO_4$ with scheelite structure and their photocatalytic properties, Chem. Mater. 13 (2001) 4624–4628.
[21] M.C. Long, W.M. Cai, J. Cai, B.X. Zhou, X.Y. Chai, Y.H. Wu, Efficient photocatalytic degradation of phenol over $Co_3O_4/BiVO_4$ composite under visible light irradiation, J. Phys. Chem. B 110 (2006) 20211–20216.
[22] J.W. Tang, Z.G. Zou, J.H. Ye, Efficient photocatalytic decomposition of organic contaminants over $CaBi_2O_4$ under visible-light irradiation, Angew. Chem. Int. Ed. 43 (2004) 4463–4466.
[23] H.B. Fu, C.S. Pan, W.Q. Yao, Y.F. Zhu, Visible-light-induced degradation of Rhodamine B by nanosized $Bi_2WO_6$, J. Phys. Chem. B 109 (2005) 22432–22439.
[24] C. Zhang, Y.F. Zhu, Synthesis of square $Bi_2WO_6$ nanoplates as high-activity visible-light-driven photocatalysts, Chem. Mater. 17 (2005) 3537–3545.
[25] Y. Shimodaira, H. Kato, H. Kobayashi, A. Kudo, Photophysical properties and photocatalytic activities of bismuth molybdates under visible light irradiation, J. Phys. Chem. B 110 (2006) 17790–17797.
[26] A. Kudo, S. Hijii, $H_2$ or $O_2$ evolution from aqueous solution on layered oxide photocatalysts consisting of $Bi^{3+}$ with $6s^2$ configuration and $d^0$ transition metal ions, Chem. Lett. 28 (1999) 1103–1104.
[27] W.F. Yao, H. Wang, X.H. Xu, J.T. Zhou, X.N. Yang, Y. Zhang, S.X. Shang, Photocatalytic property of bismuth titanate $Bi_2Ti_2O_7$, Appl. Catal. A: Gen. 259 (2004) 29–33.
[28] W.F. Yao, X.H. Xu, H. Wang, J.T. Zhou, X.N. Yang, Y. Zhang, S.X. Shang, B.B. Huang, Photocatalytic property of perovskite bismuth titanate, Appl. Catal. B: Environ. 52 (2004) 109–116.
[29] J.H. Wang, Z.G. Zou, J.H. Ye, Surface modification and photocatalytic activity of distorted pyrochlore-type $Bi_2M$ (M = In, Ga and Fe)$TaO_7$ photocatalysts, J. Phys. Chem. Solids 66 (2005) 349–355.
[30] Z.G. Zou, J.H. Ye, K. Sayama, H. Arakawa, Photocatalytic and photophysical properties of a novel series of solid photocatalysts, $BiTa_{1-x}Nb_xO_4$ ($0 \leq x \leq 1$), Chem. Phys. Lett. 343 (2001) 303–308.
[31] Z.G. Zou, J.H. Ye, H. Arakawa, Photocatalytic and photophysical properties of a novel series of solid photocatalysts, $Bi_2MNbO_7$ (M = $Al^{3+}$, $Ga^{3+}$ and $In^{3+}$), Chem. Phys. Lett. 333 (2001) 57–62.
[32] G.K. Zhang, J.L. Yang, S.M. Zhang, Q. Xiong, B.B. Huang, J.T. Wang, W.Q. Gong, Preparation of nanosized $Bi_3NbO_7$ and its visible-light photocatalytic property, J. Hazard. Mater. 172 (2009) 986–992.
[33] K. Ishibashi, A. Fujishima, T. Watanabe, K. Hashimoto, Quantum yields of active oxidative species formed on $TiO_2$ photocatalyst, J. Photochem. Photobiol. A: Chem. 134 (2000) 139–142.
[34] T. Hirakawa, Y. Nosaka, Properties of $O_2^{\bullet -}$ and $OH^{\bullet}$ formed in $TiO_2$ aqueous suspensions by photocatalytic reaction and the influence of $H_2O_2$ and some ions, Langmuir 18 (2002) 3247–3254.
[35] T. Salmi, E. Paatero, P. Nyholm, Kinetic model for the increase of reaction order during polyesterification, Chem. Eng. Proc. 43 (2004) 1487–1493.
[36] G.K. Zhang, X.M. Ding, Y.J. Hu, B.B. Huang, X.Y. Zhang, X.Y. Qin, J. Zhou, J.W. Xie, Photocatalytic degradation of 4BS dye by N,S-codoped $TiO_2$ pillared montmorillonite photocatalysts under visible-light irradiation, J. Phys. Chem. C 112 (2008) 17994–17997.
[37] N. Wang, M.Y. Zhao, Z.W. Yin, W. Li, Low-temperature synthesis of β-$BiNbO_4$ powder by citrate sol–gel method, Mater. Lett. 57 (2003) 4009–4013.
[38] D. Xie, W. Pan, H. Shi, Synthesis and characterization of $Sr_{1-x}Ba_xBi_4Ti_4O_{15}$ ferroelectric materials, Mater. Sci. Eng. B 99 (2003) 352–355.
[39] M.E. Lines, Absolute Raman intensities in glasses. I. Theory, J. Non-Cryst. Solids 89 (1987) 143–162.
[40] M.E. Lines, A.E. Miller, K. Nassau, K.B. Lyons, Absolute Raman intensities in glasses. II. Germania-based heavy metal oxides and global criteria, J. Non-Cryst. Solids 89 (1987) 163–180.
[41] D. Rusu, I. Ardelean, Structural studies of $Fe_2O_3$–$Bi_2O_3$–CdO glass system, Mater. Res. Bull. 43 (2008) 1724–1730.
[42] M.A. Butler, Photoelectrolysis and physical properties of the semiconducting electrode $WO_2$, Appl. Phys. 48 (1977) 1914–1920.
[43] A. Kudo, H. Kato, S. Nakagawa, Water splitting into $H_2$ and$O_2$ on new $Sr_2M_2O_7$ (M = Nb and Ta) photocatalysts with layered perovskite structures: factors affecting the photocatalytic activity, J. Phys. Chem. B 104 (2000) 571–575.
[44] Y. Inoue, M. Kohno, S. Ogura, K. Sato, Properties of photocatalysts with tunnel structures: formation of a surface lattice $O^-$ radical by the UV irradiation of $BaTi_4O_9$ with a pentagonal-prism tunnel structure, Chem. Phys. Lett. 267 (1997) 72–76.
[45] J.W. Tang, Z.G. Zou, J.H. Ye, Substitution effects of $Ca^{2+}$ by $Sr^{2+}$ and $Ba^{2+}$ on structural properties and photocatalytic behaviors of $CaIn_2O_4$, J. Chem. Mater. 16 (2004) 1644–1649.
[46] G.S. Shao, X.J. Zhang, Z.Y. Yuan, Preparation, photocatalytic activity of hierarchically mesoporous–macroporous $TiO_{2-x}N_x$, Appl. Catal. B: Environ. 82 (2008) 208–218.
[47] S.C. Zhang, C. Zhang, Y. Man, Y.F. Zhu, Visible light driven photocatalyst of $Bi_2WO_6$ nanoparticles prepared via amorphous complex precursor and photocatalytic properties, J. Solid State Chem. 179 (2006) 62–69.
[48] P.C. Chen, W. Lo, Molecular orbital studies of the isomers of 2,4,6-trinitrotoluene and some of its thermal decomposition products, J. Mol. Struct. 397 (1997) 21–32.
[49] P.C. Chen, W. Lo, S.C. Tzeng, Molecular structure of mononitrophenols and their thermal decomposition tautomers, J. Mol. Struct. 428 (1998) 257–266.
[50] P.C. Chen, S.C. Chen, Theoretical study of the internal rotational barriers in nitrobenzene, 2-nitrotoluene, 2-nitrophenol, and 2-nitroaniline, Int. J. Quant. Chem. 83 (2001) 332–337.
[51] H.B. Fu, L.W. Zhang, W.Q. Yao, Y.F. Zhu, Photocatalytic properties of nanosized $Bi_2WO_6$ catalysts synthesized via a hydrothermal process, Appl. Catal. B: Environ. 66 (2006) 100–110.
[52] R.C. Weast, M.J. Astle, Handbook of Chemistry and Physics, 69th ed., CRC Press Inc., Boca Raton, Florida, 1988.
[53] S. Kim, W. Choi, Kinetics and mechanisms of photocatalytic degradation of $(CH_3)_nNH_{4-n}^+$ ($0 \leq n \leq 4$) in $TiO_2$ suspension: the role of OH radicals, Environ. Sci. Technol. 36 (2002) 2019–2025.
[54] G.T. Li, J.H. Qu, X.W. Zhang, J.H. Liu, H.N. Liu, Elctrochemically assisted photocatalytic degradation of orange. II. Influence of initial pH values, J. Mol. Catal. A: Chem. 259 (2006) 238–244.
[55] S.H. Yoon, J.H. Lee, Oxidation mechanism of As(III) in the UV/$TiO_2$ system: evidence for a direct hole oxidation mechanism, Environ. Sci. Technol. 39 (2005) 9695–9701.
[56] J. Bandara, J. Kiwi, Fast kinetic spectroscopy, decoloration and production of $H_2O_2$ induced by visible light in oxygenated solutions of the azo dye orange II, New J. Chem. 23 (1999) 717–724.
[57] M. Stylidi, D. Kondarides, X. Verykios, Visible light-induced photocatalytic degradation of acid orange 7 in aqueous $TiO_2$ suspensions, Appl. Catal. B: Environ. 47 (2004) 189–201.